Nano Trends 9 (2025) 100075

Contents lists available at ScienceDirect

Nano Trends

journal homepage: www.elsevier.com/locate/nantre

Exploring the impact of modulation of electronic structure via doping in the realm of environmental applications

U Sandhya Shenoy [a,*], Bhava Amin [b], D Krishna Bhat [b,*]

[a] Department of Materials Science and Engineering, Institute of Engineering and Technology, Srinivas University, Mukka, Mangalore 574146, India
[b] Department of Chemistry, National Institute of Technology Karnataka, Surathkal, Mangalore 575025, India

ARTICLE INFO

Keywords:
Barium titanate
Silver doping
Photocatalytic dye degradation
Band gap
Solvothermal synthesis
Density functional theory

ABSTRACT

Engineering the electronic structure of a material is quite a fascinating field of study as it not only helps in improving the performance of the material but also helps us understand why a particular combination of elements exhibits the properties it does. Substitutional doping has been receiving increasing interest in the field of photocatalysis for boosting the performance of the material by tuning its crystal structure and electronic structure. In this study, we report the effect of site occupancy of silver in Ag doped $BaTiO_3$. First principles density functional theory calculations highlight that the Ti site which is the preferred site in $BaTiO_3$ for most of the dopants is not so preferred in the case of Ag doping for enhancing the photocatalytic activity. It also reveals the exceptional behavior of Ag where in it prevents the formation of mid gap recombination centers in the case of mixed occupancy. Doped samples synthesized through solvothermal approach with directed doping shows activity of 99.2 % and 99 % degradation of rose bengal and malachite green dyes in 40 and 50 min, respectively.

1. Introduction

Barium titanate, with a highly tunable crystal structure and electronic structure is emerging as a nifty material in various applications like thermoelectrics, photocatalysis, piezocatalysis and ferroelectrics [1–5]. The nontoxic, abundant, cost effective and stable nature of the perovskite type oxides has led to their study in environmental remediation [6–11]. Although these materials possess an unfavorable electronic structure with huge band gaps and recombination centers, their application in visible light photocatalytic generation of hydrogen by water splitting and degradation of pollutants is being sought, after the discovery of various strategies like doping [12–16], compositing [17–19], hetero structure formation [20,21], defect engineering[22–24] etc. which are capable of altering the properties of these materials.

Among various oxides, the perovskite titanates are the best bets as they possess multiple doping sites [25–27]. It is known that substitutional doping would modify the electronic structure based on the site the dopant occupies [1,25]. $BaTiO_3$ offers two sites viz. Ba and Ti site for cation doping and one site viz. O site for anion doping. These sites can be either individually doped or simultaneously co-doped [1,3,27–30]. Previous reports suggest that while Ce, Eu, Na, Sr, Y, Zn dopants prefer Ba site, Cr, Cu, Fe, Mn, Mo, Nb dopants prefer Ti site [2,29,31–37]. It is also known that dopants such as Rh have a tendency of creating acceptor levels when they occupy both Ba and Ti sites simultaneously, a feature also observed in its $SrTiO_3$ counterpart [3,38]. For a photocatalytic material to be highly efficient, it is necessary that the band gap be appropriately small to create an electron hole pair on absorption of visible light photon and also the electronic structure be free from mid gap states which usually acts as a site for recombination of the generated charge carriers [38]. A combination of experimental and theoretical studies have been carried out in perovskite titanates to find a touchstone for this purpose [7,9,27].

Synthetic conditions can be tailored to direct the dopant towards a particular site [3,37]. Hence, it is essential to study the changes in the electronic structure that occurs for each individual sites and for mixed occupancies. Although there are reports on synthesis of Ag doped $BaTiO_3$ using various methods like sol-gel technique, hydrothermal method, solvothermal method, spray pyrolysis, an in-depth study on the electronic structure changes with respect to site occupancies and its impact on photocatalysis have not been carried out [39–42]. Herein, for the first time we study the changes that doping of Ag in $BaTiO_3$ brings about in the electronic structure while it occupies each of the site. We reveal the unique interaction between Ag and $BaTiO_3$ which leads to mixed occupancy having the most appropriate electronic structure for

* Corresponding authors.
E-mail addresses: sandhyashenoy347@gmail.com (U.S. Shenoy), denthajekb@gmail.com (D.K. Bhat).

https://doi.org/10.1016/j.nwnano.2025.100075
Received 14 December 2024; Received in revised form 8 January 2025; Accepted 8 January 2025
Available online 9 January 2025

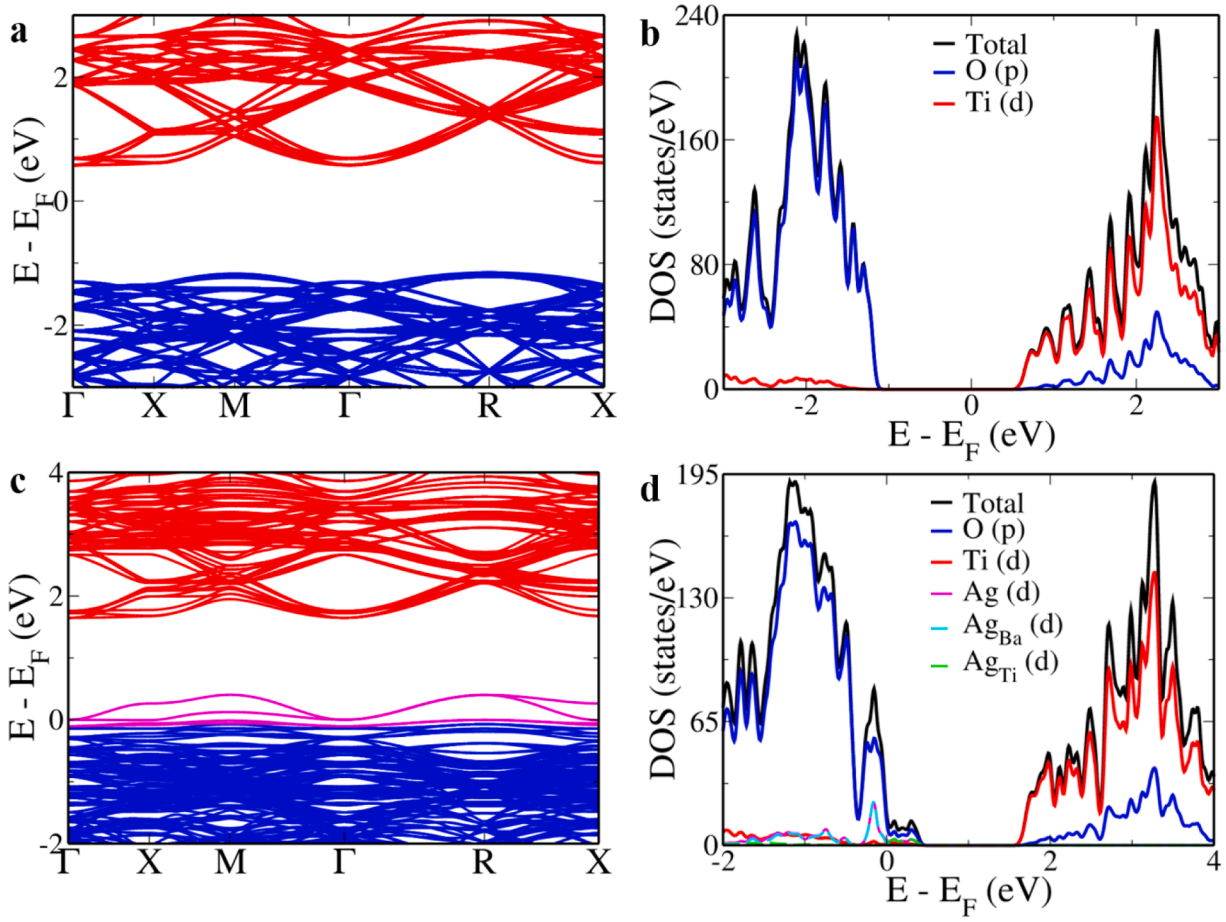

Fig. 1. Electronic structure and pdos of 3 x 3 x 3 supercell of (a and b) $BaTiO_3$; (c and d) Ag doped $BaTiO_3$ (case A) with one Ag in Ti site (indicated by green color in pDOS plot) and another Ag in Ba site (indicated by cyan color in pDOS plot).

promoting higher photocatalytic activity as opposed to the previously known fact that the mixed occupancies are a strict no-no as far as doping is considered [3,38]. We support this with experimental evidence by choosing rose Bengal (RB) and malachite green (MG) as target pollutants for photocatalytic degradation in the presence of Ag doped $BaTiO_3$ nano catalysts.

2. Methods

We conducted first principles density functional theory (DFT) simulations using the Quantum ESPRESSO package to analyze the electronic structure of both undoped and Ag doped $BaTiO_3$ [43]. The calculations were performed on a 3 × 3 × 3 supercell (135 atoms) of the primitive cubic $BaTiO_3$, with Ba atoms at the corners, Ti at the center, and O at the face centers of the cube. For the exchange and correlation energy, we used the Perdew, Burke, and Ernzerhof (PBE) functional within the generalized gradient approximation [44]. Valence electrons were modeled using ultrasoft pseudopotentials: $5s^2 5p^6 6s^2$, $3s^2 3p^6 3d^2 4s^2$, $2s^2 2p^4$, 4d $^{10}5s^1$ for Ba, Ti, O and Ag, respectively. The wave functions, represented by the plane wave basis, were truncated with energy and charge density cutoffs of 90 Ry and 720 Ry, respectively. In our calculations, a 3 × 3 × 3 k-point mesh was used for self-consistent field calculations, while a 6 × 6 × 6 mesh was employed for non-self-consistent field calculations. The electronic structure was analyzed along the high symmetry path Γ - X - M - Γ - R - X in the Brillouin zone.

$BaTiO_3$ samples in pristine and Ag-doped form were synthesized through a straightforward solvothermal process previously reported, bypassing the need for a calcination step to be carried out in addition, at high-temperature [41]. Further information on characterization details of the prepared samples is available in the supplementary material. The photocatalytic efficiency was assessed following the techniques available in literature, and additional information can be found in the supplementary materials [3,27,35].

3. Results and discussion

3.1. Electronic structure analysis

Exploring the intricacies of material electronic structure engineering is a fascinating pursuit, offering not only performance enhancement but also valuable insights into the unique properties arising from specific element combinations. The electronic structure analysis of 3 × 3 × 3 supercell of pristine $BaTiO_3$ discloses a direct band gap of 1.88 eV at the Γ point, aligning closely with previously reported values (Fig. 1a) [27, 35]. However, the band gap underestimation is a recognized phenomenon in electronic structure calculations, attributed to a discontinuity in the derivative of energy concerning the number of electrons [45]. Additionally, two indirect band gaps of 1.76 eV and 1.74 eV between M → Γ and R → Γ, respectively, are observed in the electronic structure. The partial density of states (pDOS) shown in Fig. 1b illustrates that the 'p' orbitals of oxygen and 'd' orbitals of titanium are respectively forming the valence and conduction states of undoped $BaTiO_3$ [1,46].

In this work our focus was on investigating the impact of site occupancy of silver during doping in $BaTiO_3$. For this we simulated 3 cases: (i) Case A where both Ba and Ti atoms were substituted with two Ag atoms, (ii) Case B where one Ba atom was substituted with one Ag atom and (iii) Case C where one Ti atom was substituted with one Ag atom. In

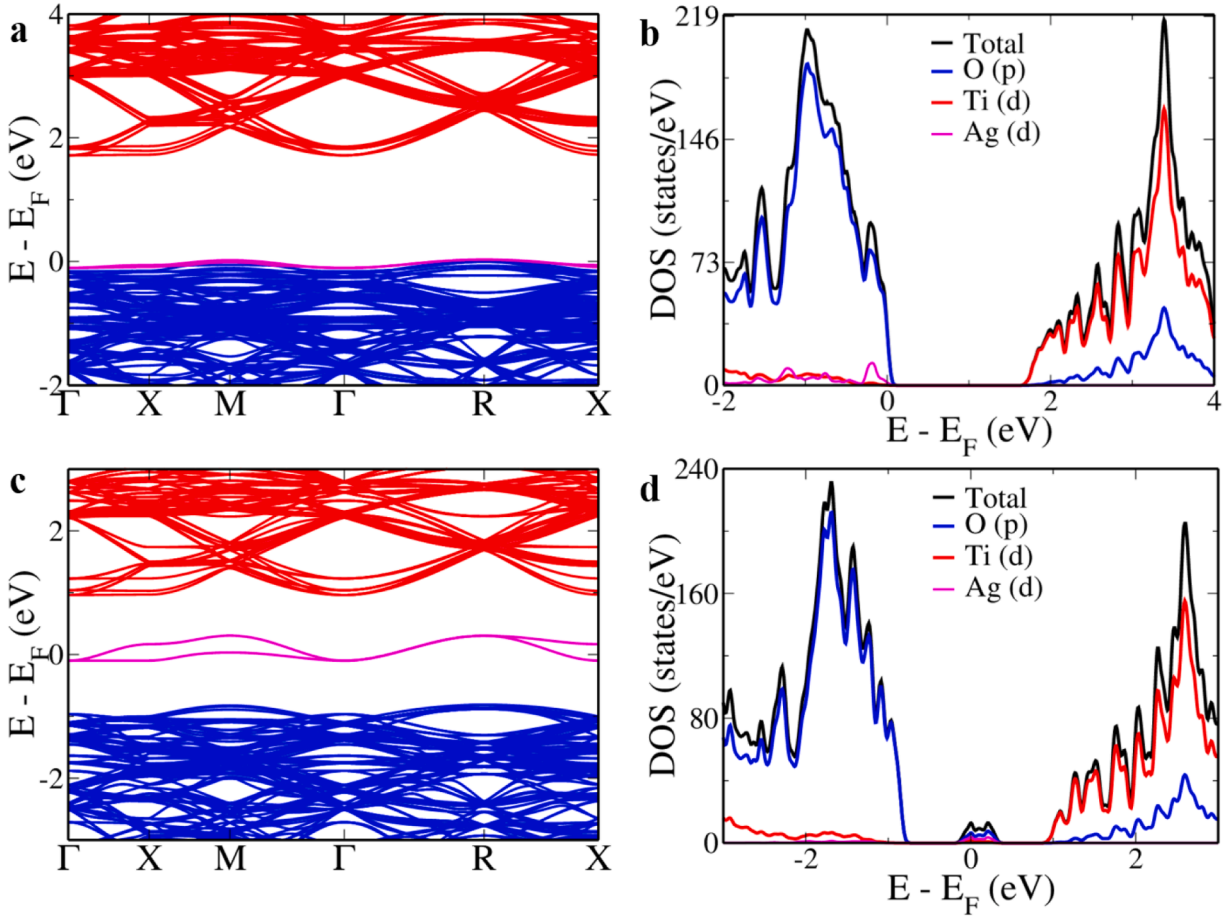

Fig. 2. Electronic structure and pdos of 3 x 3 x 3 supercell of Ag doped $BaTiO_3$ with Ag in (a and b) Ba site (case B); (c and d) Ti site (case C).

case A the direct band gap decreased to 1.65 eV at Γ point, with the indirect gaps being 1.24 eV and 1.25 eV between M → Γ and R → Γ, respectively (Fig. 1c). The pDOS depicted in Fig. 1d reveals the formation of donor states just above the valence band edge by the Ag 'd' orbitals from atom substituted at Ba site capped by the atom substituted at Ti site. This differs from the cases like Rh doping in $SrTiO_3$ and $BaTiO_3$ where mid gap states are formed due to the mixed occupancies resulting in the increased charge carrier recombination rate [3,38].

To further study if the mixed occupancy case shows the combined feature of single type site occupancy cases as revealed in previous studies of copper doping in $BaTiO_3$, we analyze electronic structures of case B and case C [27,35]. In the case B, at Γ point, we see a direct band gap measuring 1.82 eV with both the indirect gaps reducing to 1.69 eV (Fig. 2a). This slight decrement in the band gap is due to the levels introduced by the 'd' states of Ag near the valence band edge (Fig. 2b). Case C reveals a defect level at the mid gap region with a width of 0.41 eV lying 0.86 eV below the conduction band edge at Γ point (Fig. 2c). This defect band formed due to the hybridization of 'p' orbitals of O and 'd' orbitals of Ag although decreases the band gap, acts as a recombination center detrimental to the photocatalytic ability (Fig. 2d).

The key contender in harnessing solar energy for catalytic processes should possess a smaller gap, reduced recombination of charge carriers and a high surface area. The electronic structure analysis reveals that among the three cases simulated case C has the lowest band gap

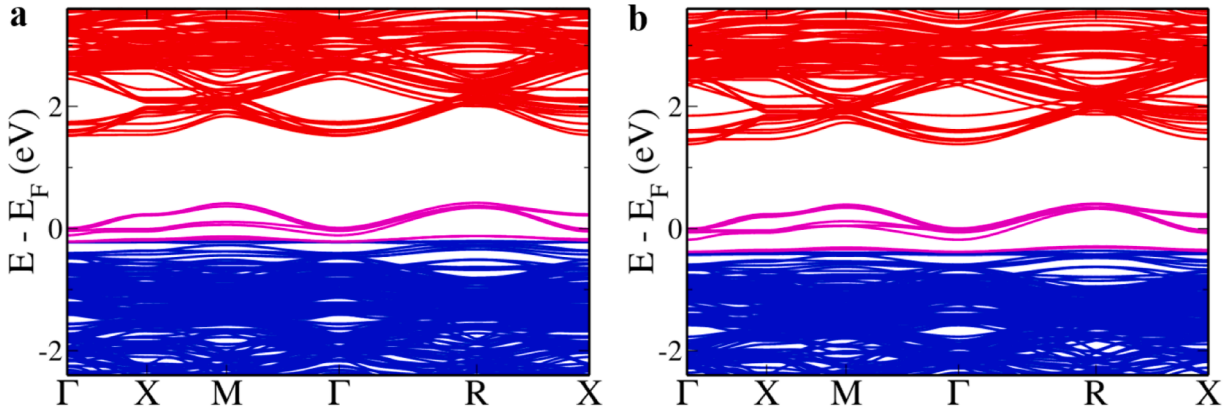

Fig. 3. Electronic structure of 3 x 3 x 3 supercell of Ag doped $BaTiO_3$ with (a) two Ag in Ti sites and one Ag in Ba site; (b) three Ag in Ti sites and one Ag in Ba site.

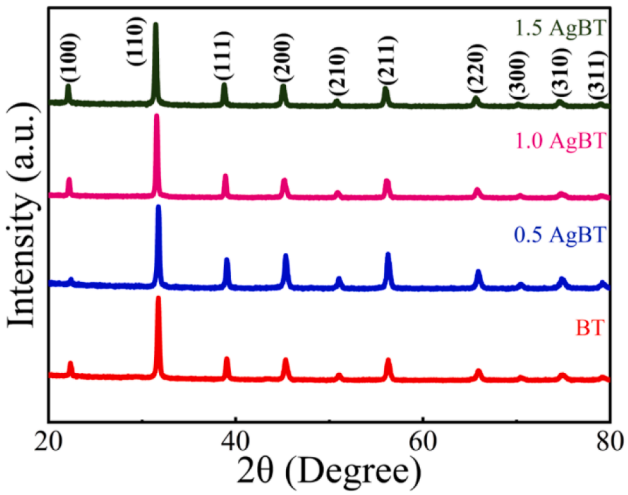

Fig. 4. XRD patterns of $BaTiO_3$ and Ag doped $BaTiO_3$ nanoparticles.

followed by case A and finally case B. Based on the band gap criteria alone materials with Ag in Ti site should perform better. But this is not the case as the acceptor states formed when Ag is substituted in Ti site provides opportunity of recombination of charge carriers thus diminishing the performance. Thus, this represents a unique case of doping contrary to the common trend, as Ti site was considered the most favorable site for many of the perovskite metal oxides for enhancing the photocatalytic performance [7,16,27,35]. We observe that when Ag shows mixed occupancy, it not only decreases the band gap to a larger extent but it also pacifies the acceptor states by dragging it closer to the valence band edge forming a continuous band with it. We further considered two cases of mixed occupancies by doping (i) two Ag in Ti sites and one Ag in Ba site and (ii) three Ag in Ti sites and one Ag in Ba site. Even in these cases of mixed occupancies we see reduction in the band gap and pacification of the acceptor states in the electronic structure (Fig. 3). To prove the hypothesis, we experimentally synthesize samples corresponding to all the three cases (A, B and C) of doping and study its photocatalytic performance in degradation of anionic and cationic dyes.

3.2. X-ray diffraction and spectroscopy analysis

The X-ray diffraction (XRD) patterns reveal the formation of pristine and Ag doped $BaTiO_3$ without any impurities, as illustrated in Fig. 4. The crystal structures align with the standard perovskite phase of $BaTiO_3$ (JCPDS card no 1–079–2263). Ba^{2+} has a co-ordination number of 12 in $BaTiO_3$, while Ti^{4+} has 6, with an ionic radius of 1.61 Å and 0.605 Å, respectively for the two cations. Ag^{+} can either have an ionic radius of 1.15 Å (for C.N. 6) or 1.28 Å (for C.N. 8). Hence, when Ag is doped into $BaTiO_3$ due to closer ionic sizes and charges it would prefer substituting Ba^{2+} while due to similar co-ordination number it may prefer Ti site also. In fact, the actual site depends on the synthetic conditions.

The lattice parameters are obtained with the help of Bragg's law using Eq. (1) for cubic system as given below:

$$d = \frac{a}{\sqrt{h^2 + k^2 + l^2}} \quad (1)$$

where h, k and l are the Miller indices of the Bragg plane, d is the grating constant and a is the lattice spacing. We see that at lower concentrations of Ag it occupies Ba site, as the concentration increases it exhibits mixed occupancies occupying both Ba and Ti sites while at higher concentrations it occupies Ti sites. This is also indicated by the change in the estimated lattice parameter 'a' of 3.99 Å for $BaTiO_3$ with Ag dopant concentrations, with the 'a' decreasing for 0.5 AgBT (3.95 Å) and increasing for 1.0 AgBT (4.00 Å) and 1.5 AgBT (4.05 Å) samples. This is further confirmed by the shift in the XRD peak of 0.5 AgBT and 1.5 AgBT towards higher and lower 2θ values, respectively compared to the pristine BT.

X-ray Photoelectron Spectroscopy (XPS) analysis furnishes insights into the elemental composition of the samples being studied. The XPS

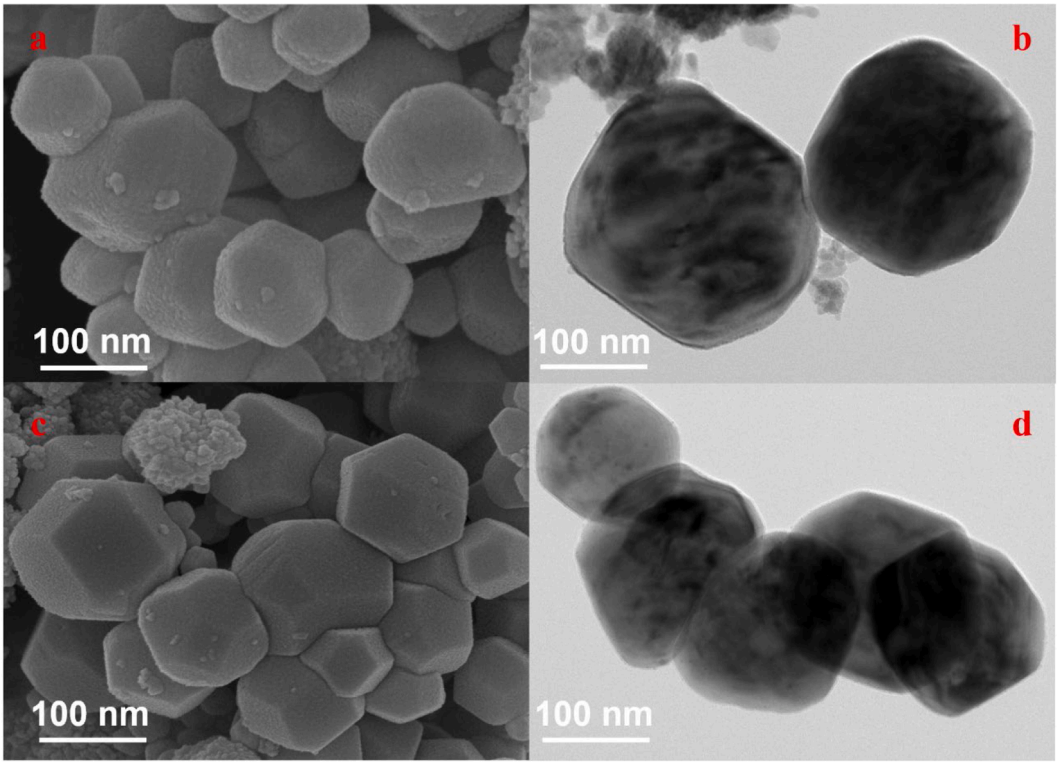

Fig. 5. FESEM and TEM image of (a and b) BT and (c and d) 1.0 AgBT.

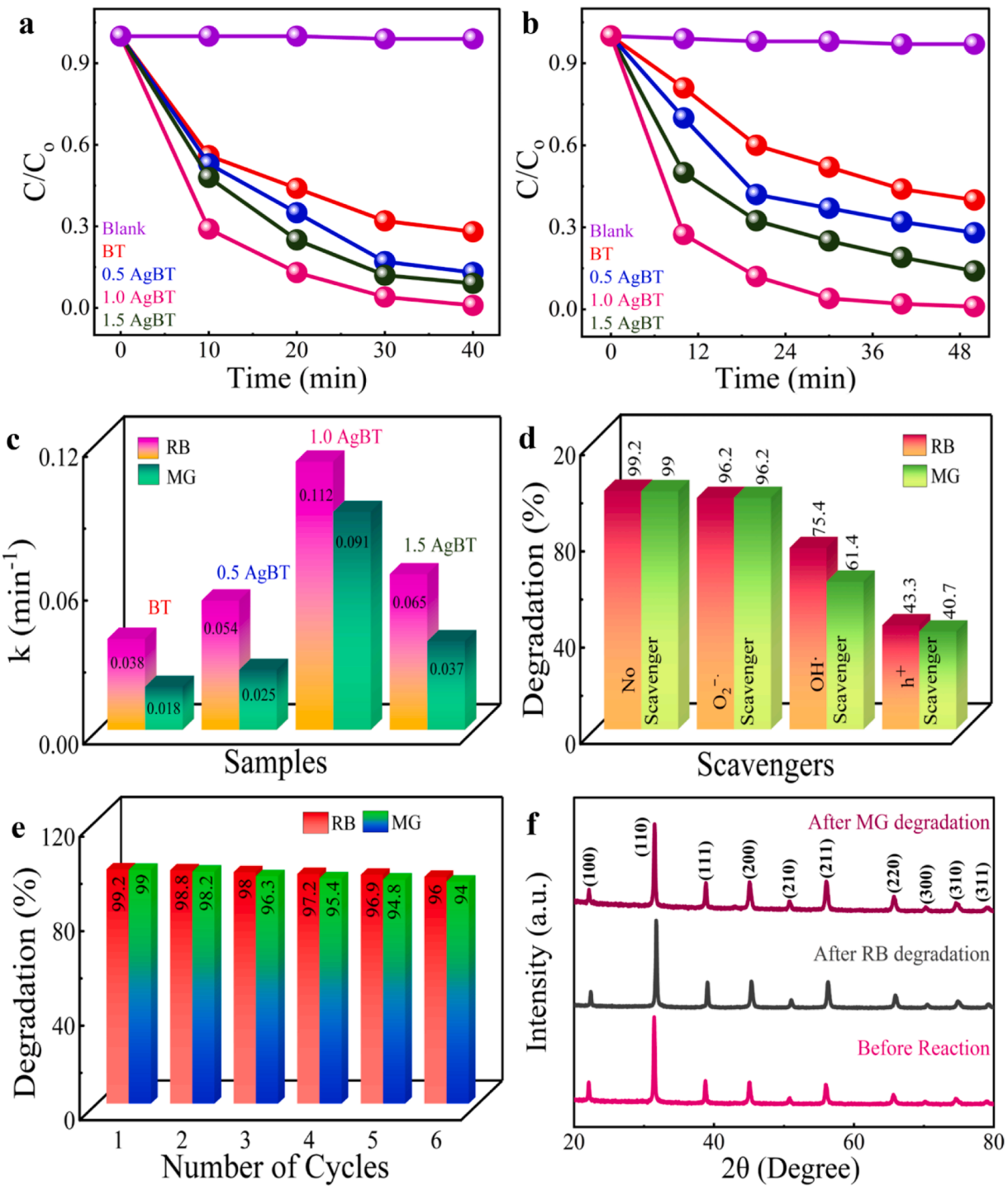

Fig. 6. Photocatalytic degradation of (a) RB and (b) MG; (c) Rate constants of the photocatalytic degradation reactions (d) Effect of radical scavengers on the photocatalytic degradation, (e) Cyclic stability test of 1.0 AgBT (f) XRD patterns of 1.0 AgBT before and after degradation of RB and MG dyes.

results reveal the presence of the elements, Ag, O, Ti, and Ba. The peaks observed at 779.3 eV and 794.6 eV binding energies correspond to the Ba $3d_{5/2}$ and Ba $3d_{3/2}$ spin states, respectively (see Figure S1a) [35]. The separation of 15.3 eV between these peaks indicates the +2 oxidation state of Ba in $BaTiO_3$ [41]. Additionally, the binding energies of 464.2 eV and 458.3 eV for Ti $2p_{1/2}$ and Ti $2p_{3/2}$ suggest that Ti is in $a + 4$ oxidation state (refer to Figure S1b) [47]. The deconvolution of silver peaks at binding energies of 373.7 eV and 367.7 eV corresponds to the Ag $3d_{3/2}$ and Ag $3d_{5/2}$ spin states, respectively (observe Figure S1c) [48, 49]. Analyses of the oxygen peaks reveals surface hydroxyl groups (O_{OH}) and lattice oxygen (O_L) identifiable by peaks at 529.7 eV and 531.5 eV binding energies, respectively (see Figure S1d) [3,41,50].

The optical properties were assessed through diffuse reflectance (DR) spectroscopy as illustrated in Figure S2a. The bandgap energy determined using the Kubelka-Munk equation shows a decreasing trend with increase in the dopant concentration supporting the results from DFT and XRD analysis regarding the site occupancy. The decrease in the band gap promotes absorption of visible light [51]. The PL analysis showed 1.0 AgBT has least intensity among all the samples (Figure S2b). The slight increase in the intensity of 1.5 AgBT indicates the presence of

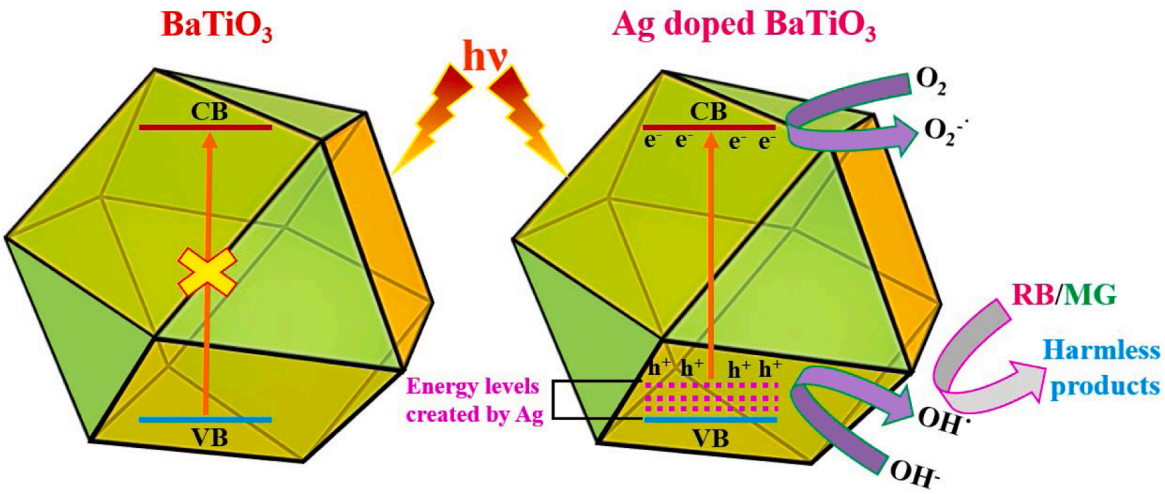

Fig. 7. The photocatalytic mechanism of the degradation of RB and MG dyes under visible light irradiation in the presence of $BaTiO_3$ and Ag doped $BaTiO_3$.

acceptor levels resulting in the formation of recombination centers supported by the DFT results and results from XRD indicating at higher dopant concentration Ag occupies Ti sites [41].

3.3. Morphology and surface area analysis

Field emission scanning electron microscopy (FESEM) and transmission electron microscopy (TEM) images captured for undoped and Ag-doped $BaTiO_3$, as depicted in Fig. 5, showcase irregularly shaped particles that tend toward a cuboctahedral structure [41]. The doped samples show clearer facets than the undoped samples. BET analysis was carried out to understand the impact of doping on surface area. The adsorption-desorption isotherms of the samples, BT and 1.0 AgBT exhibited an H3 hysteresis loop of type IV pattern, indicative of the mesoporous nature of the material (see Figure S3) [52,53]. The surface area measured for the doped and undoped $BaTiO_3$ were 35.23 m^2/g and 24.18 m^2/g, respectively. This implies that a large number of active sites are available in 1.0 AgBT, promoting an efficient adsorption followed by further degradation of pollutants [41].

3.4. Photocatalytic activity

To assess the photocatalytic activity and versatility of the catalyst, RB as a model anionic dye and MG as a model cationic dye were selected for the degradation studies under visible light conditions (Fig. 6). The degradation extent was minimal in the absence of the catalyst. Notably, 1.0 AgBT exhibited the highest degradation efficiency, reaching 99.2 % within 40 min for RB dye and 99 % within 50 min for MG dye. This superior performance can be attributed to the lower band gap and reduced rate of charge carrier recombination in the catalyst. The photocatalytic degradation of the dyes by BT and AgBT samples adhere to a pseudo first-order rate Eq. (2), given by:

$$ln(C/C_o) = -kt \quad (2)$$

where C is the concentration of the dye at irradiation time t, C_o is the initial concentration of the dye, and k is the first-order rate constant [6]. To determine the value of the rate constant k, the slope of the straight-line plot of $-\ln(C/C_o)$ versus t is utilized. Among the doped samples, 1.0 AgBT exhibited the highest rate constant [41].

Trapping experiments were conducted to identify the active species involved in the photocatalytic degradation. Benzoquinone was used to scavenge the superoxide anion radicals ($O^{2-\bullet}$), isopropyl alcohol to trap hydroxyl radicals ($OH^{\bullet}$), and EDTA to trap holes (h^+) [6,27]. Given that the 1.0 AgBT sample exhibited maximum activity, it was selected for the cyclic stability test and scavenger test. When benzoquinone was added, there was no significant change in the photocatalytic activity of the catalyst. This shows that the primary active species responsible for the degradation of the dyes are other than the superoxide radical anions. However, when EDTA and isopropyl alcohol were added, photocatalytic activity was reduced significantly. This shows that the degradation of the dyes is accomplished majorly by the holes and hydroxyl radicals [3].

To assess the reusability of the 1.0 AgBT sample, the photocatalytic activity was evaluated over 6 consecutive cycles. The catalyst exhibited minimal reduction in photocatalytic degradation efficiency during the test, demonstrating ample stability for practical applications in water treatment as an environmentally friendly photocatalyst. To investigate whether the photocatalyst's structure underwent any changes during the degradation reaction, the XRD pattern of 1.0 AgBT was examined after the reactions. The XRD pattern remained unchanged after the degradation reaction, indicating the structural stability of the catalyst. Comparison of the photocatalytic activity of 1.0 AgBT with the previously reported materials reveal that the synthesized material reported here is highly efficient (Table S1).

Based on the presented results, a proposed photodegradation mechanism for the dyes is depicted in Fig. 7. Light absorption initiates the generation of charge carriers, where electrons from the valence band (VB) transition to the conduction band (CB), creating holes (h^+) in the VB. The electrons in the CB are then engaged by oxygen to generate anionic superoxide radicals. Simultaneously, the holes in the VB either directly react with the dye or undergo a reaction with water to produce hydroxyl radicals ($OH^{\bullet}$), which further react with dye molecules, degrading them into harmless products by attacking the aromatic rings [3,6,27].

4. Conclusions

The present work reports a holistic approach of combining computational and experimental techniques to enhance the photocatalytic performance of $BaTiO_3$ by doping Ag. We delve into the impact of site occupancy during doping of silver in $BaTiO_3$ using first principles calculations within density functional theory. Contrary to the common trend where the Ti site is favored for most dopants in enhancing the photocatalytic activity in $BaTiO_3$, our findings reveal a distinct preference in the case of Ag doping. Surprisingly, Ag exhibits exceptional behavior by averting the formation of mid-gap recombination centers with mixed occupancy. Experimental synthesis of doped samples using a solvothermal approach, with careful attention to directed doping, demonstrates notable photocatalytic activity. The doped samples exhibit 99.2 % and 99 % degradation efficiency for rose bengal and malachite

green, respectively, within 40 and 50 min. Our findings emphasize the importance of careful composition optimization for Ag doped $BaTiO_3$ nanoparticles to achieve enhanced photocatalytic activity, offering promising applications in water treatment and environmental remediation.

CRediT authorship contribution statement

U Sandhya Shenoy: Writing – review & editing, Writing – original draft, Methodology, Investigation, Funding acquisition, Conceptualization. **Bhava Amin:** Investigation. **D Krishna Bhat:** Writing – review & editing, Supervision, Software, Resources, Project administration, Formal analysis, Conceptualization.

Declaration of competing interest

The authors declare that they have no known competing financial interests or personal relationships that could have appeared to influence the work reported in this paper.

Acknowledgement

The author (USS) gratefully acknowledges the financial support received from Science and Engineering Research Board, Department of Science and Technology, Government of India under SERB Research Scientist scheme.

Supplementary materials

Supplementary material associated with this article can be found, in the online version, at doi:10.1016/j.nwnano.2025.100075.

References

[1] U.S. Shenoy, D.K. Bhat, Vanadium-doped $BaTiO_3$ as high performance thermoelectric material: role of electronic structure engineering, Mater. Today Chem. 18 (2020) 100384.
[2] X. Xiao, M. Widenmeyer, W. Xie, T. Zou, S. Yoon, M. Scavini, S. Checchia, Z. Zhong, P. Hansmann, S. Kilper, A. Kovalevsky, A. Weidenkaff, Tailoring the structure and thermoelectric properties of $BaTiO_3$ via Eu^{2+} substitution, Phys. Chem. Chem. Phys. 19 (2017) 13469–13480.
[3] D.K. Bhat, H. Bantawal, U.S. Shenoy, Rhodium doping augments photocatalytic activity of barium titanate: effect of electronic structure engineering, Nanoscale Adv. 2 (2020) 5688–5698.
[4] Q. Zhang, Y. Jia, W. Wu, C. Pei, G. Zhu, Z. Wu, L. Zhang, W. Fan, Z. Wu, Review on strategies toward efficient piezocatalysis of $BaTiO_3$ nanomaterials for wastewater treatment through harvesting vibration energy, Nano Energy 113 (2023) 108507.
[5] B. Jiang, J. Iocozzia, L. Zhao, H. Zhang, Y.W. Harn, Y. Chen, Z. Lin, Barium titanate at the nanoscale: controlled synthesis and dielectric and ferroelectric properties, Chem. Soc. Rev. 48 (2019) 1194–1228.
[6] D.K. Bhat, P.I. Uma, U.S. Shenoy, Exceptional light harvesting in copper doped $CaTiO_3$ nanocuboids with surface nanosteps for the photo remediation of toxic Cr (VI) ions and dyes, *J. Alloys Compd. Commun.* 4 (2024) 100030.
[7] H. Bantawal, U.S. Shenoy, D.K. Bhat, Vanadium doped $CaTiO_3$ cuboids: role of vanadium in improving the photocatalytic activity, Nanoscale Adv 3 (2021) 5301–5311.
[8] J. Wang, C. Hu, L. Shi, N. Tian, H. Huang, H. Ou, Y. Zhang, Energy and environmental catalysis driven by stress and temperature-variation, J. Mater. Chem. A 9 (2021) 12400–12432.
[9] P.I. Uma, U.S. Shenoy, D.K. Bhat, Nanocubic copper-doped $SrTiO_3$ for photoreduction of Cr(VI) and photodegradation of methyl violet, ACS Appl. Nano Mater. 6 (2023) 16798–16804.
[10] L. Jing, Y. Xu, M. Xie, Z. Li, C. Wu, H. Zhao, J. Wang, H. Wang, Y. Yan, N. Zhong, H. Li, J. Hu, Piezo-photocatalysts in the field of energy and environment: designs, applications, and prospects, Nano Energy 112 (2023) 108508.
[11] D.K. Bhat, H. Bantawal, P.I. Uma, S.P. Kumar, U.S. Shenoy, Designing sustainable porous graphene-$CaTiO_3$ nanocomposite for environmental remediation, Sustain. Chem. Environ. 5 (2024) 100071.
[12] P. Xie, F. Yang, R. Li, C. Ai, C. Lin, S. Lin, Improving hydrogen evolution activity of perovskite $BaTiO_3$ with Mo doping: experiments and first-principles analysis, Int. J. Hydrog. Energy 44 (2019) 11695–11704.
[13] P. Senthilkumar, D.A. Jency, T. Kavinkumar, D. Dhayanithi, S. Dhanuskodi, M. Umadevi, S. Manivannan, N.V. Giridharan, V. Thiagarajan, M. Sriramkumar, K. Jothivenkatachalam, Built-in electric field assisted photocatalytic dye degradation and photoelectrochemical water splitting of ferroelectric Ce doped $BaTiO_3$ nanoassemblies, ACS Sustain. Chem. Eng. 7 (2019) 12032–12043.
[14] D.K. Bhat, P.I. Uma, U.S. Shenoy, Insights into the dopant engineering in copper-doped $SrTiO_3$ nanocubes, J. Hazard. Mater. Adv. 12 (2023) 100380.
[15] B.D. Kavey, D. Caruntu, V. Mykhailovych, G. Caruntu, Ferroelectric monodisperse Ln-doped barium titanate cuboidal nanocrystals prepared by a solvothermal route, CrystEngComm 24 (2022) 7089–7102.
[16] H. Bantawal, U.S. Shenoy, D.K. Bhat, Vanadium-doped $SrTiO_3$ nanocubes: insight into role of vanadium in improving the photocatalytic activity, Appl. Surf. Sci. 513 (2020) 145858.
[17] H. Jiao, X. Zhou, S. Song, J. Jin, X. Zhang, Y. Tang, K. Zhao, Barium titanate (101)/silver nanocomposite: preparation, photocatalytic activity, and mechanism based on density functional theory, Mat. Sci. Eng. B 288 (2023) 116137.
[18] D.K. Bhat, H. Bantawal, P.I. Uma, U.S. Shenoy, Enhanced photoresponse and efficient charge transfer in porous graphene-$BaTiO_3$ nanocomposite for high performance photocatalysis, Diam. Relat. Mater. 139 (2023) 110312.
[19] H. Bantawal, M. Sethi, U.S. Shenoy, D.K. Bhat, Porous graphene wrapped $SrTiO_3$ nanocomposite: Sr–C bond as an effective coadjutant for high performance photocatalytic degradation of methylene blue, ACS Appl. Nano Mater. 2 (2019) 6629–6636.
[20] S. Wang, Q. Li, K. Ge, Y. Yang, Y. Zhang, M. Pan, L. Zhu, Ferroelectric nano-heterojunctions for piezoelectricity-enhanced photocatalysis, Sep. Purif. Technol. 305 (2023) 122433.
[21] R. Su, Z. Sun, C. He, S. Wei, L. Chen, D. Zhang, Z. Wang, X. An, F. Li, Engineering heterostructured $Ti_4O_5/BaTiO_3$ ferroelectric by surface reconstruction for enhanced photocatalytic CO_2 reduction, Inorg. Chem. Front. 10 (2023) 3947–3954.
[22] H. Arandiyan, S.S. Mofarah, C.C. Sorrell, E. Doustkhah, B. Sajjadi, D. Hao, Y. Wang, H. Sun, B.J. Ni, M. Rezaei, Z. Shao, T. Maschmeyer, Defect engineering of oxide perovskites for catalysis and energy storage: synthesis of chemistry and materials science, Chem. Soc. Rev. 50 (2021) 10116–10211.
[23] H. Bantawal, U.S. Shenoy, D.K. Bhat, Tuning the photocatalytic activity of $SrTiO_3$ by varying the Sr/Ti ratio: unusual effect of viscosity of the synthesis medium, J. Phys. Chem. C 122 (2018) 20027–20033.
[24] X. Wang, S. Ma, B. Liu, S. Wang, W. Huang, Imperfect makes perfect: defect engineering of photoelectrodes towards efficient photoelectrochemical water splitting, Chem. Commun. 59 (2023) 10044–10066.
[25] U.S. Shenoy, D.K. Bhat, Electronic structure engineering of $SrTiO_3$ via rhodium doping: a DFT study, J. Phys. Chem. Solids 148 (2021) 109708.
[26] Y. Fo, X. Zhou, A theoretical study on tetragonal $BaTiO_3$ modified by surface co-doping for photocatalytic overall water splitting, Int. J. Hydrog. Energy 47 (2022) 19073–19085.
[27] P.I. Uma, U.S. Shenoy, D.K. Bhat, Doped $BaTiO_3$ cuboctahedral nanoparticles: role of copper in photocatalytic degradation of dyes, Appl. Surf. Sci. 15 (2023) 100408.
[28] I.C. Amaechi, A. Hadj Youssef, D. Rawach, J.P. Claverie, S. Sun, A. Ruediger, Ferroelectric Fe–Cr codoped $BaTiO_3$ nanoparticles for the photocatalytic oxidation of azo dyes, ACS Appl. Nano Mater. 2 (2019) 2890–2901.
[29] Y.J. Choi, S.W. Kim, T.L. Phan, B.W. Lee, D.S. Yang, Tetragonal-structural changes influenced the magnetic and ferroelectric properties of (Y, Fe)-codoped $BaTiO_3$ ceramics, Curr. Appl. Phys. 53 (2023) 39–45.
[30] U.S. Shenoy, D.K. Bhat, Enhanced thermoelectric properties of vanadium doped $SrTiO_3$: a resonant dopant approach, J. Alloys Compd. 832 (2020) 154958.
[31] H. Gao, Y. Zhang, H. Xia, X. Zhu, X. Mao, W. Zhao, S. Miao, M. Shi, In situ generation of H_2O_2 over Ce-doped $BaTiO_3$ catalysts for enhanced piezo-photocatalytic degradation of pollutants in aqueous solution, Colloids Surf. A Physicochem. Eng. Asp. 663 (2023) 131030.
[32] S.M. Yakout, Influence of Na and Na/Fe doping on the dielectric constant, ferromagnetic and sunlight photocatalytic properties of $BaTiO_3$ perovskite, J. Solid State Chem. 290 (2020) 121517.
[33] B. Yang, H. Chen, Y. Yang, L. Wang, J. Bian, Q. Liu, X. Lou, Insights into the tribo-/pyro-catalysis using Sr-doped $BaTiO_3$ ferroelectric nanocrystals for efficient water remediation, Chem. Eng. J. 416 (2021) 128986.
[34] J.P. Zou, L.Z. Zhang, S.L. Luo, L.H. Leng, X.B. Luo, M.J. Zhang, Y. Luo, G.C. Guo, Preparation and photocatalytic activities of two new Zn-doped $SrTiO_3$ and $BaTiO_3$ photocatalysts for hydrogen production from water without cocatalysts loading, Int. J. Hydrog. Energy 37 (2012) 17068–17077.
[35] P.I. Uma, U.S. Shenoy, D.K. Bhat, Electronic structure engineering of $BaTiO_3$ cuboctahedrons by doping copper to enhance the photocatalytic activity for environmental remediation, J. Alloys Compd. 948 (2023) 169600.
[36] I.C. Amaechi, A. Hadj Youssef, G. Kolhatkar, D. Rawach, C. Gomez-Yañez, J. P. Claverie, S. Sun, A. Ruediger, Ultrafast microwave-assisted hydrothermal synthesis and photocatalytic behaviour of ferroelectric Fe^{3+}-doped $BaTiO_3$ nanoparticles under simulated sunlight, Catal. Today 360 (2021) 90–98.
[37] D. Phuyal, S. Mukherjee, S. Jana, F. Denoel, M.V. Kamalakar, S.M. Butorin, A. Kalaboukhov, H. Rensmo, O. Karis, Ferroelectric properties of $BaTiO_3$ thin films co-doped with Mn and Nb, AIP Adv 9 (2019) 095207.
[38] U.S. Shenoy, H. Bantawal, D.K. Bhat, Band engineering of $SrTiO_3$: effect of synthetic technique and site occupancy of doped rhodium, J. Phys. Chem. C 122 (2018) 27567–27574.
[39] M. Zhang, J. Zheng, L. Liang, F. Jiang, Y. Wang, Preparation and microwave absorption properties of Ag doped $BaTiO_3$ nanocomposites, J. Magn. Magn. Mater. 368 (2014) 198–201.
[40] E. Lin, Z. Kang, J. Wu, R. Huang, N. Qin, D. Bao, $BaTiO_3$ nanocubes/cuboids with selectively deposited Ag nanoparticles: efficient piezocatalytic degradation and mechanism, Appl. Cat. B: Environ. 285 (2021) 119823.
[41] A. Bhava, U.S. Shenoy, D.K. Bhat, Silver doped barium titanate nanoparticles for enhanced visible light photocatalytic degradation of dyes, Environ. Pollut. 344 (2024) 123430.

[42] Y.N. Ko, Y.C. Kang, Characteristics of Ag doped $BaTiO_3$ nanopowders prepared by spray pyrolysis, Ceram. Int. 38 (2012) 2071–2077.
[43] P. Giannozzi, S. Baroni, N. Bonini, M. Calandra, R. Car, C. Cavazzoni, D. Ceresoli, G.L. Chiarotti, M. Cococcioni, I. Dabo, A. Dal Corso, S. de Gironcoli, S. Fabris, G. Fratesi, R. Gebauer, U. Gerstmann, C. Gougoussis, A. Kokalj, M. Lazzeri, L. Martin-Samos, N. Marzari, F. Mauri, R. Mazzarello, S. Paolini, A. Pasquarello, L. Paulatto, C. Sbraccia, S. Scandolo, G. Sclauzero, A.P. Seitsonen, A. Smogunov, P. Umari, R.M. Wentzcovitch, QUANTUM ESPRESSO: a modular and open-source software project for quantum simulations of materials, J. Phys. Condens. Matter 21 (2009) 395502.
[44] J.P. Perdew, K. Burke, M. Ernzerhof, Generalized gradient approximation made simple, Phys. Rev. Lett. 77 (1996) 3865–3868.
[45] U.S. Shenoy, D.K. Bhat, Molybdenum as a versatile dopant in SnTe: a promising material for thermoelectric application, Energy Adv 1 (2022) 9–14.
[46] Y. Fo, Y. Ma, H. Dong, X. Zhou, Tuning the electronic structure of $BaTiO_3$ for an enhanced photocatalytic performance using cation–anion codoping: a first-principles study, New J. Chem. 45 (2021) 8228–8239.
[47] U.S. Shenoy, P.I. Uma, D.K. Bhat, Copper doping induced band structure and morphology transformation in $CaTiO_3$ for textile dye photodegradation applications, J. Alloys Compd. 1004 (2024) 175779.
[48] J.H. Li, B.F. Yan, X.S. Shao, S.S. Wang, H.Y. Tian, Q.Q. Zhang, Influence of Ag/TiO_2 nanoparticle on the surface hydrophilicity and visible-light response activity of polyvinylidene fluoride membrane, Appl. Surf. Sci. 324 (2015) 82–89.
[49] Y. Wang, H. Yang, X. Sun, H. Zhang, T. Xian, Preparation and photocatalytic application of ternary n-$BaTiO_3$/Ag/p-AgBr heterostructured photocatalysts for dye degradation, Mater. Res. Bull. 124 (2020) 110754.
[50] Z. Zhu, J. Ye, X. Tang, Z. Chen, J. Yang, P. Huo, Y.H. Ng, J. Crittenden, Vacancy-rich CoS_x@LDH@Co-NC catalytic membrane for antibiotic degradation with mechanistic insights, Environ. Sci. Technol. 57 (2023) 16131–16140.
[51] Q. Qi, W. Shen, M. Cai, J. Cai, B. Hu, D. Han, X. Tang, Z. Zhi, P. Huo, Construction of Cu-Modified g C_3N_4 Nanosheets for Photoinduced CO_2 Reduction to CO and Selectivity Mechanism Insight, ACS Appl. Nano Mater. 7 (2024) 24788–24797.
[52] M. Sethi, U.S. Shenoy, D.K. Bhat, Porous graphene-$NiCo_2O_4$ nanorod hybrid composite as a high performance supercapacitor electrode material, New J. Chem. 44 (2020) 4033–4041.
[53] Z. Zhu, X. Xing, Q. Qi, W. Shen, H. Wu, D. Li, B. Li, J. Liang, X. Tang, J. Zhao, H. Li, P. Huo, Fabrication of graphene modified CeO_2/g-C_3N_4 heterostructures for photocatalytic degradation of organic pollutants, Chinese J. Struct. Chem. 42 (2023) 100194.